EFFECT OF AI CONTENT ON THE MICROSTRUCTURE, MICROHARDNESS AND CORROSION RESISTANCE OF AI_xCoCrFeNiMo_{0.5} HIGH-ENTROPY ALLOYS

Olga Samoilova¹, Svetlana Pratskova^{1,2}, Nataliya Shaburova¹, Ahmad Ostovari Moghaddam^{1,3}, Sergey Lezhnev⁴, Evgeniy Panin⁵, Evgeny Trofimov¹

¹South Ural State University, Chelyabinsk, Russia, samoilovaov@susu.ru (O.S.);

se_pratskova@mail.ru (S.P.); shaburovana@susu.ru (N.S.);

ostovarim@susu.ru (A.O.M.); trofimovea@susu.ru (E.T.);

Received 15 February 2025 Accepted 02 March 2025

DOI: 10.59957/jctm.v60.i6.2025.21

ABSTRACT

The microstructure, microhardness and corrosion resistance (in a 1 M NaCl) of as-cast Al_x CoCrFeNi $Mo_{0.5}$ (x=0,0.25,0.5) high-entropy alloys (HEAs) were studied. The as-cast samples exhibited a dendritic microstructure in which a (CrFeMo)-type molybdenum-rich σ -phase precipitated in the interdendritic space. It was determined that Al alloying increases the microhardness from 285 $HV_{0.3}$ for CoCrFeNi $Mo_{0.5}$ HEA to 628 $HV_{0.3}$ for $Al_{0.5}$ CoCrFeNi $Mo_{0.5}$ HEA. At the same time, aluminium has a negative effect on the corrosion resistance of the studied alloys, where an increase in Al concentration, increases the corrosion current by two orders of magnitude.

Keywords: high entropy alloys, microstructure, microhardness, corrosion.

INTRODUCTION

High-entropy alloys (HEAs) have attracted much attention from material scientists in the last two decades, after the pioneer works published by Cantor and Yeh in 2004 [1, 2]. To large extend, this is due to the unique combination of mechanical properties and tribological characteristics in HEAs [3 - 9]. Moreover, Al_xCoCrFeNi HEAs are among the most promising corrosion-resistant materials [10 - 13]. Currently, studies on the effect of additionally introduced elements on the properties of Al_xCoCrFeNi HEAs are still ongoing.

Zhuang et al. reported a significant positive effect of molybdenum on the mechanical properties of Al_{0.5}CoCrFeMo_xNi HEAs [14]. On the other hand, molybdenum is proven as an alloying element that increases corrosion resistance and reduces pitting in various types of steel in salt solutions [15, 16].

Therefore, Mo can be considered as a promising element to increase corrosion resistance of HEAs. For example, Chou et al. demonstrated that the simultaneous presence of Ti and Mo in Co_{1.5}CrFeNi_{1.5}Ti_{0.5}Mo_x HEA not only increases its corrosion resistance but also reduces its pitting in a 1M NaCl solution [17]. Rodriguez et al. showed that molybdenum increases the passivation range of a HEA in 3.5 wt. % NaCl solution compared to a similar Mo-free composition and several industrial alloys [18]. Based on the results of tests in acidic and Cl-containing solutions, Wang et al. reported that Mo-containing HEAs exhibit excellent resistance to localized corrosion [19].

However, to use Mo-containing HEAs as construction materials or protective coatings, it is necessary to find a composition with an optimal combination of mechanical properties and corrosion resistance. There are only a few works devoted to research in this area. For example, Löbel et al studied the

²Chelyabinsk State University, Chelyabinsk, Russia

³HSE University, 101000 Moscow, Russia

⁴Rudny Industrial University, Rudny, Kazakhstan, sergey legnev@mail.ru (S.L.)

⁵Karaganda Industrial University, Temirtau, Kazakhstan, cooper802@mail.ru (E.P.)

effect of co-alloying of aluminium and molybdenum on the characteristics of Al_{0.3}CrFeCoNiMo_{0.2} coating [20]. It was shown that aluminium increases microhardness of the coating, and molybdenum helps to reduce the corrosion current density, slows down pitting corrosion, and consequently, improves corrosion resistance. On the other hand, the positive effect of Mo on the mechanical characteristics of HEAs only begins at sufficiently high concentrations of Mo [14, 21 - 23]. This demonstrates that there is still a scientific gap on the combined effect of Al and Mo on the characteristics of HEAs.

Therefore, this work aims to study the effect of aluminium concentration on the characteristics of $Al_xCoCrFeNiMo_{0.5}$ (x = 0, 0.25, 0.5) HEAs. The microstructure, microhardness, and corrosion resistance of the as-cast alloys in a 1 M NaCl solution is studied.

EXPERIMENTAL

Al_xCoCrFeNiMo_{0.5} (x = 0, 0.25, 0.5) HEAs ingots were fabricated by induction melting at 1700-1750°C in vacuum using metals (granules and powders manufactured JSC "POLEMA", Tula, Russia) of high purity (> 99.9 wt. %). Three re-melts were performed to obtain a homogeneous microstructure and to avoid molybdenum segregation.

The microstructure was examined using a JSM-7001F scanning electron microscope (SEM) (JEOL, Tokyo, Japan) equipped with an energy dispersive detector (EDS) (Oxford Instruments, Abingdon, UK) for quantitative chemical analysis. X-ray diffraction (XRD) was carried out on an Ultima IV diffractometer (Rigaku, Tokyo, Japan) using Cu Kα radiation. Microhardness measurements were performed using an FM-800 microhardness tester (Future-Tech Corp., Tokyo, Japan) at a load of 300 g, the holding time was 10 s.

Corrosion tests were carried out in a 1M NaCl solution. The working electrodes for electrochemical tests were prepared from as-cast HEAs ingots as described in our previous work [24]. The nominal composition of the samples and the exposed free surface areas of the working electrodes are presented in Table 1. Polarization measurements were performed in a standard three-electrode YaSE-2 electrochemical

cell (OJSC "Gomel Plant of Measuring Instruments", Gomel, Belarus) with a platinum counter electrode using a potentiostat-galvanostat P-45X (Electrochemical instruments, Chernogolovka, Russia). The potentials were measured with respect to a saturated silver chloride electrode at a temperature 25°C. The scanning rate of the potential for recording the full Tafel dependences was 1 mV s⁻¹.

The open circuit potential $E_{\rm OCP}$ (Table 1) was measured for 60 min. Corrosion parameters such as corrosion potential ($E_{\rm corr}$) and current density ($I_{\rm corr}$) were determined by Tafel extrapolation method using both the cathodic and anodic branches of the polarization curves. Also, the passivation current density ($I_{\rm pass}$) and the passivation potential range (ΔE) were determined from the type of polarization curves. All potentials were recalculated to the scale of a normal hydrogen electrode.

RESULTS AND DISCUSSION

Fig. 1 shows the microstructure of the as-cast $Al_xCoCrFeNiMo_{0.5}$ (x = 0, 0.25, 0.5) HEAs. The microstructure has a pronounced dendritic character for all three studied compositions. Dendrites (D) are enriched in Co and Ni (Table 2), and the phase with an increased Mo content is in the interdendritic space (ID or ID1). For $Al_{0.5}CoCrFeNiMo_{0.5}$ HEA, an additional phase containing increased concentrations of Al and Ni (ID2) was found in the interdendritic space. These microstructural observations indicate that Al affects the wettability of the primary dendrite crystals by melt during crystallization. For Al-free sample, the precipitation of a Mo-containing phase is discontinuous, which indicates incomplete wettability.

Table 1. Nominal chemical formula, electrodes surface area, and open circuit potentials.

HEA	Working surface area, mm ²	E _{OCP} , V (in 1M NaCl)
CoCrFeNiMo _{0.5}	12.24	+0.005
Al _{0.25} CoCrFeNiMo _{0.5}	12.84	-0.125
Al _{0.5} CoCrFeNiMo _{0.5}	12.73	-0.075

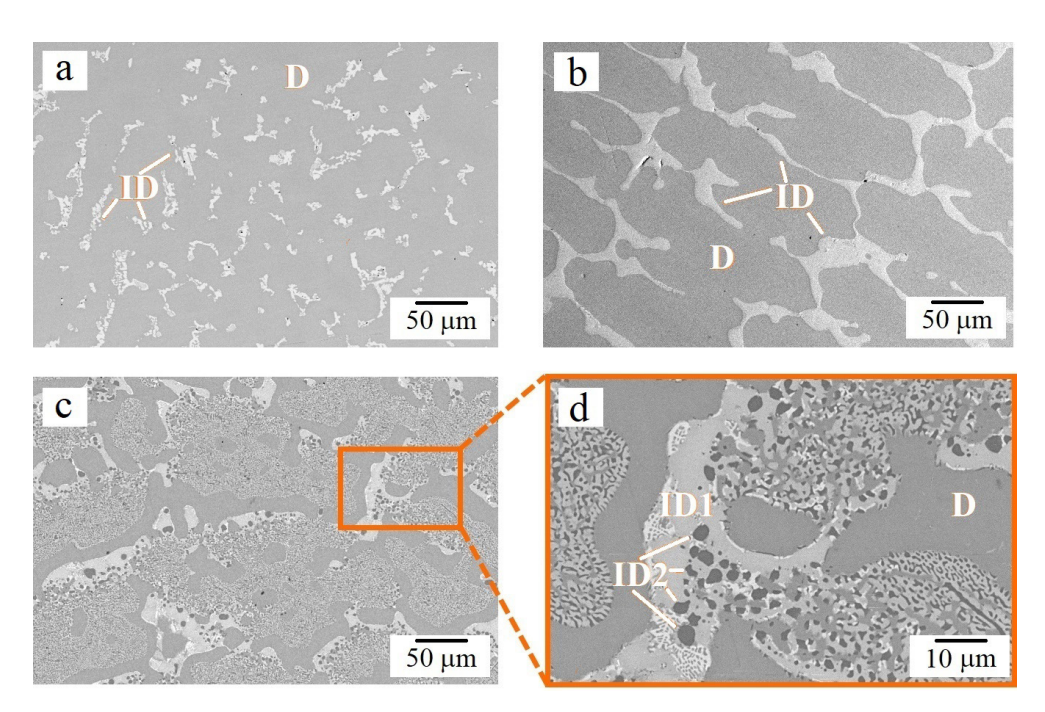


Fig. 1. SEM (back-scattered electrons mode) micrographs of the as-cast HEAs: (a) CoCrFeNiMo_{0.5}; (b) $Al_{0.25}$ CoCrFeNiMo_{0.5}; (c, d) $Al_{0.5}$ CoCrFeNiMo_{0.5}.

Table 2. Chemical composition (EDS, at. %) of the as-cast HEAs. Av (average composition), D (dendrite), and ID (interdendritic space).

HEA		Al	Co	Cr	Fe	Ni	Mo
CoCrFeNiMo _{0.5}	Av	-	22.35	22.48	22.38	22.08	10.71
	D	-	25.24	18.89	24.64	24.25	6.98
	ID	-	11.46	29.34	20.55	12.85	25.80
Al _{0.25} CoCrFeNiMo _{0.5}	Av	5.01	21.30	21.25	21.21	21.39	9.84
	D	6.21	23.13	18.27	22.62	23.43	6.34
	ID	2.26	12.63	28.89	20.88	11.57	23.77
Al _{0.5} CoCrFeNiMo _{0.5}	Av	9.54	20.14	20.55	20.23	20.11	9.43
	D	9.49	22.78	17.46	22.17	21.86	6.24
	ID1	4.63	13.56	28.24	20.68	9.74	23.15
	ID2	33.78	16.16	6.43	11.23	31.52	0.88

While the samples with aluminum in their composition are characterized by continuous separation of dendrites by interdendritic layers, and, accordingly, complete wettability. The morphology of the microstructural components affects the properties of the bulk material, as detailed elsewhere [25, 26].

Configurational entropy of mixing can be determined according to the Eq. (1) [27]:

$$\Delta S_{\text{mix}} = -R \sum_{i=1}^{n} X_i \ln X_i'$$
(1)

where R is the universal gas constant (R = 8.314 Jmol⁻¹K⁻¹),andXistheatomicfractionoftheelements. When $\Delta S_{mix} \geq 1.5 R$, the system can be considered as a high entropy. Using the average chemical composition data in Table 2, the values of the configurational entropy of mixing were obtained as $\Delta S_{mix} = 1.58 R$ for CoCrFeNiMo_{0.5}, $\Delta S_{mix} = 1.7 R$ for Al_{0.25}CoCrFeNiMo_{0.5}, and $\Delta S_{mix} = 1.74 R$ for Al_{0.5}CoCrFeNiMo_{0.5}. Thus, all three compositions can be classified as high-entropy alloys.

XRD patterns of the as-cast samples (Fig. 2) show

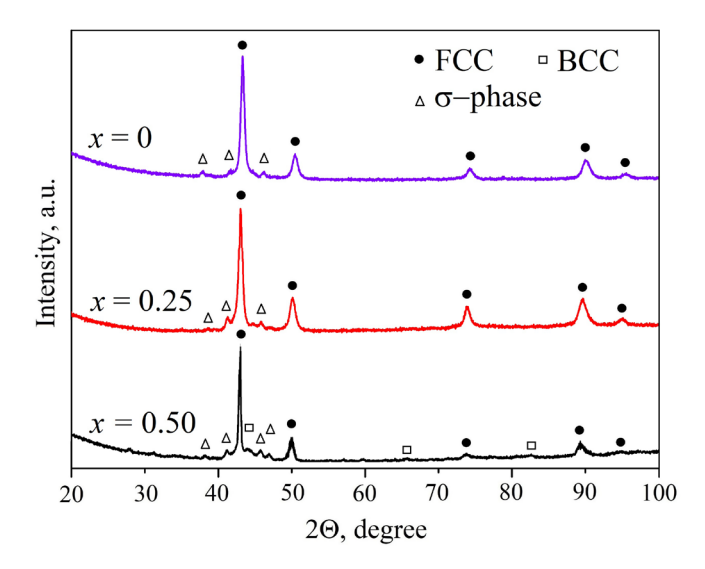


Fig. 2. X-ray diffraction pattern of the as-cast Al_xCoCrFeNiMo_{0.5} HEA samples.

diffraction from fcc solid solution, (CrFeMo)-type σ -phase, and a bcc solid solution at high aluminium content of x=0.5. The presence of the σ -phase corresponds to the phase diagrams of the Fe-Mo, Fe-Cr, and the unlimited solubility in Cr-Mo binary system in both liquid and solid states [28 - 30]. In addition, precipitation of the σ -phase in as-cast Mocontaining HEAs has been already reported in previous studies [14, 19, 21 - 23]. The appearance of a bcc solid solution at high aluminium content in HEA also does not contradict the literature data [31 - 33].

Considering microstructural features and diffraction patterns of the as-cast HEAs, the dendrites can be attributed to the fcc solid solution, interdendritic layers with a high molybdenum content (ID or ID1) can be defined as the σ -phase, and ID2 precipitates are bcc solid solution.

Fig. 3 shows microhardness values of the as-cast samples. By increasing aluminum content from x = 0 to x = 0.25, the microhardness of the samples increases by 30 %, and when the aluminium content reaches x = 0.5, the microhardness increases twofold. This effect can be associated with the solid-solution strengthening effect of aluminium in the fcc solid solution and the appearance of a bcc solid solution in the microstructure of the $Al_{0.5}$ CoCrFeNiMo_{0.5} alloy.

The microhardness value obtained for $Al_{0.5}CoCrFeNiMo_{0.5}$ HEA (628 HV) is near to that

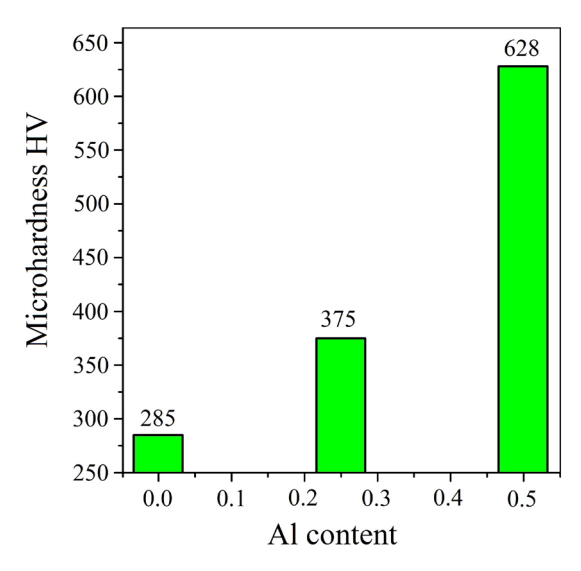


Fig. 3. Microhardness of the as-cast Al_x CoCrFeNiMo_{0.5} HEA samples.

reported by Zhuang et al., where a value of 571 HV is given for $Al_{0.5}CoCrFeMo_{0.5}Ni$ HEA [14]. Löbel et al. determined a microhardness of 400 \pm 20 HV for $Al_{0.3}CrFeCoNiMo_{0.2}$ coating, which is comparable with the values obtained in this study for CoCrFeNiMo_{0.5} (285 HV) and $Al_{0.25}CoCrFeNiMo_{0.5}$ (375 HV) samples [20].

According to the polarization curves (Fig. 4), anodic control is the characteristic of corrosion behaviour of all three samples. It is obvious that aluminium reduces the corrosion resistance of the studied alloys in a 1 M NaCl (Table 3). With an increase in aluminium content from x = 0 to x = 0.5, the corrosion potential significantly shifts to the negative side, the corrosion current increases by two orders of magnitude, and the passivation area decreases by half.

Also, to assess the corrosion resistance of alloys in an aqueous solution containing chlorine ions, polarization resistance (R_p) was further calculated using Eq. (2):

$$R_{p} = \frac{1}{2.303 \left(\frac{1}{\beta_{a}} + \frac{1}{\beta_{c}}\right) I_{corr}},$$
(2)

where β_a and β_c are the slope coefficients of the anode and cathode straight lines of the Tafel equation, respectively, obtained by extrapolation. The results

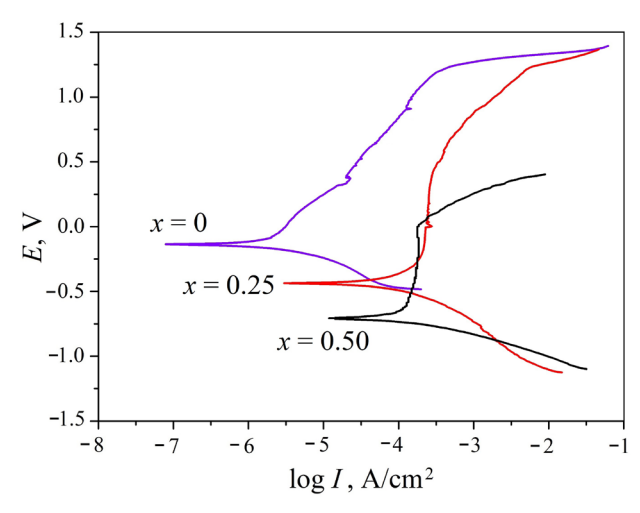


Fig. 4. Polarization curves of the as-cast Al $_x$ CoCrFeNiMo $_{0.5}$ HEA samples in 1M NaCl solution.

of the calculation of the polarization resistance are given in Table 3. For CoCrFeNiMo_{0.5}, the polarization resistance index is two orders of magnitude higher than that of the other two samples, which confirms the presence of a passivating film with excellent protective properties on its surface.

The morphological features of the electrode surfaces

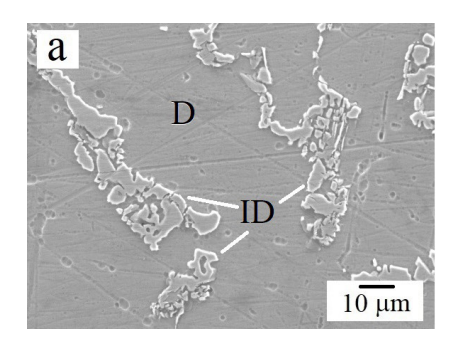
after testing (Fig. 5) confirm the obtained results. Moreover, the corroded surface of CoCrFeNiMo_{0.5} and Al_{0.25}CoCrFeNiMo_{0.5} HEAs does not show any damage and is relatively even and smooth, while the corroded surface of Al_{0.5}CoCrFeNiMo_{0.5} sample is characterized by selective dissolution of the aluminium-rich ID2 phase, and clearly visible corrosion pits.

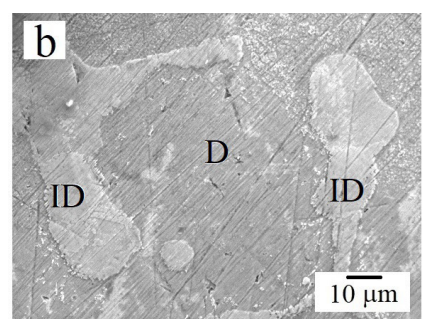
EDS was conducted on the corroded surfaces (Table 4), oxygen concentration confirms the changes detailed above. It is also necessary to pay attention to the concentration of chlorine, which is the highest on the surface of Al_{0.5}CoCrFeNiMo_{0.5} sample, and it is known that chlorine-containing corrosion products contribute to the destruction of the passivating film and reduce its protective properties [35].

Comparing the chemical composition of the samples before and after corrosion test (Tables 2, 4), it is noted that the average chemical composition of the surface changes after corrosion test. The content of Al, Fe, Co and Ni decreases, while the concentration of Cr and Mo increases or remains unchanged. This can be attributed to the opening of the internal alloy layers during corrosion, as selective dissolution of the surface layer occurs. Analysis of the data shows

Table 3. Potentials and current densities of alloys in a 1M NaCl.

Alloy	E _{corr} ,	I _{corr} , μA cm ⁻²	I _{pass} , μA cm ⁻²	ΔE, V	R_{p} , $k\Omega \text{ cm}^{2}$
CoCrFeNiMo _{0.5}	-0.135	0.23	76	1.294	33.09
Al _{0.25} CoCrFeNiMo _{0.5}	-0.435	8.95	251	0.764	0.88
Al _{0.5} CoCrFeNiMo _{0.5}	-0.702	15.68	173	0.664	0.49
Co _{1.5} CrFeNi _{1.5} Ti _{0.5} [17]	-0.443	0.57	1.46	0.557	-
Co _{1.5} CrFeNi _{1.5} Ti _{0.5} Mo _{0.1} [17]	-0.381	0.13	3.80	1.429	-
Co _{1.5} CrFeNi _{1.5} Ti _{0.5} Mo _{0.5} [17]	-0.493	0.20	4.10	1.383	-
Co _{1.5} CrFeNi _{1.5} Ti _{0.5} Mo _{0.8} [17]	-0.551	0.41	5.11	1.371	-
Al _{0.5} CoCrFeNi _{1.6} Ti _{0.7} [24]	-0.626	16.2	132	0.730	2.93
Al _{0.45} CoCrFeNiSi _{0.45} [24]	-0.340	8.0	93	0.570	1.86
Al _{0.25} CoCrFeNiCu [24]	-0.401	8.6	109	0.278	3.89
AlCrFeNiCoCu [34]	-0.012	0.003	-	0.525	-
SS 304 [34]	-0.238	0.35	-	-	-
Al _{0.25} CoCrFeNiCu _{0.25} [35]	-0.802	19.7	280	1.020	0.55
Al _{0.25} CoCrFeNiCu _{0.25} Au _{0.1} [35]	-0.799	5.1	200	1.030	2.75
Al _{0.25} CoCrFeNiCu _{0.25} Au _{0.3} [35]	-0.763	5.8	90	1.070	4.48





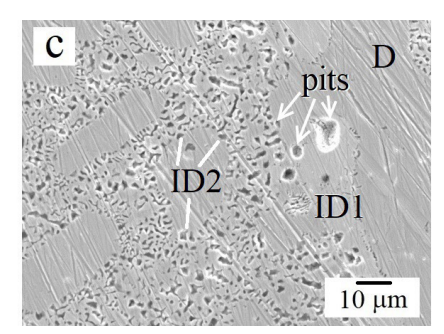


Fig. 5. SEM (secondary electrons mode) micrographs of the surface of HEA samples after corrosion test in 1M NaCl solution: (a) CoCrFeNiMo_{0.5}; (b) Al_{0.5}CoCrFeNiMo_{0.5}; (c) Al_{0.5}CoCrFeNiMo_{0.5}.

Table 4. Chemical composition (EDS, at. %) of the surface of the HEA samples after corrosion test in a 1 M NaCl solution. Av - average composition; D - dendrite; ID - interdendritic space.

HEA		Al	Co	Cr	Fe	Ni	Mo	О	C1
CoCrFeNiMo _{0.5}	Av	-	21.72	23.36	21.73	19.66	11.06	2.35	0.12
	D	-	23.24	20.74	23.33	20.73	7.89	3.84	0.23
	ID	-	12.70	29.86	19.35	12.27	25.40	0.39	0.03
Al _{0.25} CoCrFeNiMo _{0.5}	Av	3.34	17.67	20.66	17.33	17.51	11.54	11.83	0.12
	D	4.35	18.03	18.96	18.52	18.20	8.25	13.52	0.17
	ID	2.01	10.70	24.66	19.88	10.65	23.77	8.26	0.07
Al _{0.5} CoCrFeNiMo _{0.5}	Av	5.01	16.55	19.52	16.46	16.63	10.11	15.51	0.21
	D	6.46	16.86	17.26	15.20	17.54	8.03	18.28	0.37
	ID1	2.96	10.46	23.29	19.21	8.10	21.66	14.22	0.10

that areas enriched in molybdenum are subject to less corrosion. This confirms the thesis that molybdenum and chromium increase the corrosion resistance of the HEA in a solutions containing chloride ions.

CONCLUSIONS

The effect of aluminium content on the microstructure, microhardness and corrosion resistance of $Al_x CoCrFeNiMo_{0.5}$ (x = 0, 0.25, 0.5) HEAs was studied. With increasing aluminium content, the microstructure becomes more complex and upon reaching x = 0.5, in addition to fcc dendrites and Morich σ -phase interdendritic layers, islands of a bcc solid solution with increased content of Al and Ni are found in the microstructure. Such a microstructure provides the highest microhardness and the lowest corrosion resistance in a 1M NaCl. Based on our results, it can be noted that the optimal combination of mechanical characteristics and corrosion resistance is obtained in a composition with aluminium content in the range of 0 < x < 0.25.

Acknowledgements

The study was supported by the Russian Science Foundation, project No. 23-23-00107, https://rscf.ru/en/project/23-23-00107/.

Authors' contributions: O.S.: methodology, investigation, writing-original draft; S.P.: investigation, funding acquisition, project administration; N.Sh.: validation, data curation; A.O.M.: visualization, investigation; S.L.: conceptualization, methodology, investigation; E.P.: formal analysis, resources; E.T.: software, writing - review end editing.

REFERENCES

- B. Cantor, I.T.H. Chang, P. Knight, A.J.B. Vincent, Microstructural development in equiatomic multicomponent alloys, Mater. Sci. Eng. A, 375-377, 2004, 213-218. https://doi.org/10.1016/j. msea.2003.10.257
- 2. J.W. Yeh, S.K. Chen, S.J. Lin, J.Y. Gan, T.S. Chin,

- T.T. Shun, C.H. Tsau, S.Y. Chang, Nanostructured high-entropy alloys with multiple principal elements: Novel alloy design concepts and outcomes, Adv. Eng. Mater., 6, 2004, 299-303. https://doi.org/10.1002/adem.200300567
- Z. Li, K.G. Pradeep, Y. Deng, D. Raabe, C.C. Tasan, Metastable high-entropy dual-phase alloys overcome the strength-ductility trade-off, Nature, 534, 2016, 227-230. https://doi.org/10.1038/ nature17981
- E.P. George, W.A. Curtin, C.C. Tasan, High entropy alloys: A focused review of mechanical properties and deformation mechanisms, Acta Mater., 188, 2020, 435-474. https://doi.org/10.1016/j. actamat.2019.12.015
- M. Seifi, D. Li, Z. Yong, P.K. Liaw, J.J. Lewandowski, Fracture toughness and fatigue crack growth behavior of as-cast high-entropy alloys, JOM, 67, 2015, 2288-2295. https://doi. org/10.1007/s11837-015-1563-9
- M.A. Hemphill, T. Yuan, G.Y. Wang, J.W. Yeh, C.W. Tsai, A. Chuang, P.K. Liaw, Fatigue behavior of Al_{0.5}CoCrCuFeNi high entropy alloys, Acta Mater., 60, 2012, 5723-5734. https://doi.org/10.1016/j.actamat.2012.06.046
- Y. Liu, S. Ma, M.C. Gao, C. Zhang, T. Zhang, H. Yang, Z. Wang, J. Qiao, Tribological properties of AlCrCuFeNi₂ high-entropy alloy in different conditions, Metall. Mater. Trans. A, 47, 2016, 3312-3321. https://doi.org/10.1007/s11661-016-3396-8
- A.K. Kasar, K. Scalaro, P.L. Menezes, Tribological properties of high-entropy alloys under dry conditions for a wide temperature range - A review, Materials, 14, 2021, 5814. https://doi.org/10.3390/ ma14195814
- O. Samoilova, N. Shaburova, A. Ostovari Moghaddam, E. Trofimov, Al_{0.25}CoCrFeNiSi_{0.6} high entropy alloy with high hardness and improved wear resistance, Materials Letters, 328, 2022, 133190. https://doi.org/10.1016/j. matlet.2022.133190
- 10. Y. Shi, B. Yang, P.K. Liaw, Corrosion-resistant high-entropy alloys: A review, Metals, 7, 2017, 43. https://doi.org/10.3390/met7020043
- Y. Qiu, S. Thomas, M.A. Gibson, H.L. Fraser,
 N. Birbilis, Corrosion of high entropy alloys,
 NPJ Mater. Degrad., 1, 2017, 15. https://doi.

- org/10.1038/s41529-017-0009-y
- 12. Q.H. Li, T.M. Yue, Z.N. Guo, X. Lin, Microstructure and corrosion properties of AlCoCrFeNi high entropy alloy coatings deposited on AISI 1045 steel by the electrospark process, Metall. Mater. Trans. A, 44A, 2013, 1767-1778. https://doi.org/10.1007/s11661-012-1535-4
- Y. Shi, B. Yang, X. Xie, J. Brechtl, K.A. Dahmen, P.K. Liaw, Corrosion of AlxCoCrFeNi highentropy alloys: Al-content and potential scan-rate dependent pitting behavior, Corrosion Science, 119, 2017, 33-45. https://doi.org/10.1016/j. corsci.2017.02.019
- Y.X. Zhuang, X.L. Zhang, X.Y. Gu, Effect of molybdenum on phases, microstructure and mechanical properties of Al_{0.5}CoCrFeMo_xNi high entropy alloys, Journal of Alloys and Compounds, 743, 2018, 514-522. https://doi.org/10.1016/j.jallcom.2018.02.003
- S.-B. Shin, S.-J. Song, Y.-W. Shin, J.-G. Kim, B.-J. Park, Y.-C. Suh, Effect of molybdenum on the corrosion of low alloy steels in synthetic seawater, Materials Transactions, 57, 2016, 2116-2121. https://doi.org/10.2320/matertrans.M2016222
- H.-Y. Ha, T.-H. Lee, J.-H. Bae, D.W. Chun, Molybdenum effects on pitting corrosion resistance of FeCrMnMoNC austenitic stainless steels, Metals, 8, 2018, 653. https://doi.org/10.3390/ met8080653
- Y.L. Chou, J.W. Yeh, H.C. Shih, The effect of molybdenum on the corrosion behaviour of the high-entropy alloys Co_{1.5}CrFeNi_{1.5}Ti_{0.5}Mo_x in aqueous environments, Corr. Sci., 52, 2010, 2571-2581. https://doi.org/10.1016/j.corsci.2010.04.004
- 18. A.A. Rodriguez, J.H. Tylczak, M.C. Gao, P.D. Jablonski, M. Detrois, M. Ziomek-Moroz, J.A. Hawk, Effect of molybdenum on the corrosion behavior of high-entropy alloys CoCrFeNi₂ and CoCrFeNi2Mo_{0.25} under sodium chloride aqueous conditions, Advances in Materials Science and Engineering, 2018, 2018, 3016304. https://doi.org/10.1155/2018/3016304
- X. Wang, D. Mercier, Y. Danard, T. Rieger, L. Perrière, M. Laurent-Brocq, I. Guillot, V. Maurice, P. Marcus, Enhanced passivity of Cr-Fe-Co-Ni-Mo multi-component single-phase face-centred cubic alloys: design, production and corrosion

- behavior, Corros. Sci., 200, 2022, 110233. https://doi.org/10.1016/j.corsci.2022.110233
- 20. M. Löbel, T. Lindner, M. Grimm, L.-M. Rymer, T. Lampke, Influence of aluminum and molybdenum on the microstructure and corrosion behavior of thermally sprayed high-entropy alloy coatings, J Therm. Spray Tech., 31, 2022, 1366-1374. https://doi.org/10.1007/s11666-021-01297-6
- C.-Y. Hsu, T.-S. Sheu, J.-W. Yeh, S.-K. Chen, Effect of iron content on wear behavior of AlCoCrFe_xMo_{0.5}Ni high-entropy alloys, Wear, 268, 2010, 653-659. https://doi.org/10.1016/j. wear.2009.10.013
- 22. J.M. Zhu, H.M. Fu, H.F. Zhang, A.M. Wang, H. Li, Z.Q. Hu, Microstructures and compressive properties of multicomponent AlCoCrFeNiMo alloys, Materials Science and Engineering A, 527, 2010, 6975-6979. https://doi.org/10.1016/j.msea.2010.07.028
- Y. Dong, Y. Lu, J. Kong, J. Znang, T. Li, Microstructure and mechanical properties of multicomponent AlCrFeNiMo_x high-entropy alloys, Journal of Alloys and Compounds, 573, 2013, 96-101. https://doi.org/10.1016/j.jallcom.2013.03.253
- 24. S. Pratskova, O. Samoilova, E. Ageenko, N. Shaburova, A. Ostovari Moghaddam, E. Trofimov, Corrosion resistance of Al_xCoCrFeNiM (M = Ti, V, Si, Mn, Cu) high entropy alloys in NaCl and H₂SO₄ solutions, Metals, 12, 2022, 352. https://doi.org/10.3390/met12020352
- 25. B. Straumal, I. Konyashin, WC-Based cemented carbides with high entropy alloyed binders: A review, Metals, 13, 2023, 171. https://doi.org/10.3390/met13010171
- B. Straumal, N. Khrapova, A. Druzhinin, K. Tsoy, G. Davdian, V. Orlov, G. Gerstein, A. Straumal, Grain boundary wetting transition in the Mg-based ZEK 100 alloy, Crystals, 13, 2023, 1538. https://doi.org/10.3390/cryst13111538

- 27. R.A. Swalin, Thermodynamics of Solids, New York, Wiley, 1972.
- 28. A.F. Guillermet, The Fe-Mo (iron-molybdenum) system, Bulletin of Alloy Phase Diagrams, 3, 1982, 359-367. https://doi.org/10.1007/BF02869315
- 29. A. Jacob, E. Povoden-Karadeniz, E. Kozeschnik, Revised thermodynamic description of the Fe-Cr system based on an improved sublattice model of the σ phase, Calphad, 60, 2018, 16-28. https://doi.org/10.1016/j.calphad.2017.10.002
- M. Venkatraman, J.P. Neumann, The Cr-Mo (chromium-molybdenum) system, Bulletin of Alloy Phase Diagrams, 8, 1987, 216-220. https:// doi.org/10.1007/BF02874911
- 31. W.-R. Wang, W.-L. Wang, J.-W. Yeh, Phases, microstructure and mechanical properties of Al_xCoCrFeNi high-entropy alloys at elevated temperatures, J. Alloys Compd., 589, 2014, 143-152. https://doi.org/10.1016/j.jallcom.2013.11.084
- 32. M. Ogura, T. Fukushima, R. Zeller, P.H. Dederichs, Structure of the high-entropy alloy Al_xCrFeCoNi: fcc versus bcc, J. Alloys Compd., 715, 2017, 454-459. https://doi.org/10.1016/j.jallcom.2017.04.318
- 33. S. Abbaszadeh, A. Pakseresht, H. Omidvar, A. Shafiei, Investigation of the high-temperature oxidation behavior of the Al0.5CoCrFeNi high entropy alloy, Surf. Interf., 21, 2020, 100724. https://doi.org/10.1016/j.surfin.2020.100724
- 34. X.W. Qiu, Microstructure and properties of AlCrFeNiCoCu high entropy alloy prepared by powder metallurgy, J. Alloys Compd., 555, 2013, 246-249. https://doi.org/10.1016/j.jallcom.2012.12.071
- 35. O.V. Samoilova, S.E. Pratskova, N.A. Shaburova, E.A. Trofimov, Electrochemical behavior of Al_{0.25}CoCrFeNiCu_{0.25}Au_x (x = 0; 0.1; 0.3) highentropy alloys in an aqueous solution of sodium chloride, ChemChemTech, 67, 9, 2024, 27-34. https://doi.org/10.6060/ivkkt.20246709.6986